Published in final edited form as:
J Pharm Sci. 2010 January ; 99(1): 82–93. doi:10.1002/jps.21797.

Understanding and modulating opalescence and viscosity in a monoclonal antibody formulation

Branden A Salinas[1,3], **Hasige A Sathish**[1,3,4], **Steven M Bishop**[4], **Nick Harn**[4], **John F Carpenter**[2,3], and **Theodore W Randolph**[1,3]

[1] Department of Chemical and Biological Engineering, University of Colorado, Boulder, Colorado

[2] University of Colorado Health Sciences Center, Denver, Colorado

[3] Center for Pharmaceutical Biotechnology, University of Colorado

[4] MedImmune, LLC. Gaithersburg, MD 20878

Abstract

Opalescence and high viscosities can pose challenges for high concentration formulation of antibodies. Both phenomena result from protein-protein intermolecular interactions that can be modulated with solution ionic strength. We studied a therapeutic monoclonal antibody that exhibits high viscosity in solutions at low ionic strength (~20 centipoise (cP) at 90 mg/mL and 23°C) and significant opalescence at isotonic ionic strength (approximately 100 nephelometric turbidity units at 90 mg/mL and 23°C). The intermolecular interactions responsible for these effects were characterized using membrane osmometry, static light scattering and zeta potential measurements. The net protein-protein interactions were repulsive at low ionic strength (~4 mM) and attractive at isotonic ionic strengths. The high viscosities are attributed to electroviscous forces at low ionic strength and the significant opalescence at isotonic ionic strength is correlated with attractive antibody interactions. Furthermore there appears to be a connection to critical phenomena and it is suggested that the extent of opalescence is dependent on the proximity to the critical point. We demonstrate that by balancing the repulsive and attractive forces via intermediate ionic strengths and by increasing the mAb concentration above the apparent critical concentration both opalescence and viscosity can be simultaneously minimized.

Introduction

For the treatment of chronic conditions with therapeutic proteins, patient-administered delivery via subcutaneous injection is preferable.[1] Subcutaneous administration imposes a volume restriction of less than 1.5 mL, which in the case of some proteins, and particularly antibodies, requires protein concentrations that can surpass 100 mg/mL.[2] In addition to accelerated aggregation rates at high protein concentrations,[3] high-concentration antibody formulations may exhibit undesirable opalescence and high viscosity.[4,5,6]

Opalescence introduces a potential safety issue because an opalescent solution is easily confused with turbid solutions which can result from protein aggregation or other particulate formation. Furthermore, it is challenging to develop placebo formulations for clinical studies that match the opalescence of the original protein formulation. Opalescence can arise in solutions that do not contain particulates; the cloudy appearance is simply a result of Rayleigh scattering.[4] Proteins are typically Rayleigh scatterers of visible light as they have diameters of less than 30 nm.

Likewise, the high viscosities that can be exhibited by antibody solutions introduce several challenges. Manufacturing processes such as increasing protein concentration or buffer

exchange with tangential flow filtration may become infeasible. Also, the force and time required for subcutaneous injection of viscous formulations can result in increased pain on injection or even preclude this route of delivery altogether.[5]

Protein-protein interactions play important roles in both viscosity and opalescence of protein solutions. Sukumar et al describe how attractive mAb interactions can lead to opalescent solutions in the absence of any significant association between protein molecules.[4] The opalescence is attributed to a simple intermolecular attraction though this may be an oversimplification as it appears that the proximity to the liquid-liquid phase boundary and/or the critical point is important.[7] Liu et al detail an example of a monoclonal antibody that reversibly self-associates and thus generates higher viscosity solutions relative to two non-associating mAbs.[6,8]

Moon et al., Yousef et al. and Minton have all used membrane osmometry to characterize the physical behavior of model proteins such as bovine serum albumin and lysozyme at concentrations above 400 mg/mL.[9,10,11] Osmometry is particularly amenable to high concentration studies as it is not subject to the optical limitations of other techniques such as analytical ultracentrifugation or light scattering. Various methods of interpreting osmotic pressure data have been developed. In the case of Moon et al. the protein-protein interactions are characterized via second virial coefficients for a binary protein mixture at concentrations up to 100 mg/mL.[9] Minton has presented a hard particle model for characterizing the osmotic pressures of proteins such as BSA and ovalbumin to concentrations above 400 mg/mL.[11,12,13] Ross and Minton have also developed a model for the viscosity of protein solutions at high concentrations by applying the Mooney equation for hard-spheres to proteins.[14] Yousef et al. characterized the osmotic pressure of BSA and an IgG up to concentrations above 400 mg/mL with a free-solvent model that reveals information about protein hydration and protein-ion interactions.[10,15]

Light scattering is a complimentary method to membrane osmometry for determination of second virial coefficients as it reveals information about protein molecular weight and net protein-protein interactions in the given solvent. The second virial coefficient can be divided into a number of contributing components but is primarily influenced by hard-sphere repulsion, electrostatic repulsion or attraction and van der Waals attractions.[16] When measured with osmometry or light scattering, the second virial coefficient appears to include influences of cosolutes on protein nonideality.[17] Thus, it should not be considered a measure of only protein-protein interactions as suggested by the standard statistical-mechanical definition of second virial coefficients, but rather an overall indication of the protein's nonideality in solution.[17] Even so, second virial coefficients from osmometry or light scattering measurements provide a useful parameter that has a statistical-mechanical basis and that is predictive of phase behavior and other events that derive from protein nonideality in solution.[17]

Because of their long-range nature, electrostatic forces are expected to be a dominant influence on the intermolecular interactions responsible for opalescence and viscosity of protein solutions at pH values where the protein retains a significant effective charge. Ionic strength influences protein solution viscosities as well as the positions of solution phase boundaries and cloud points by modulating the electrostatic contribution to the intermolecular potential.[5,6,18] In order to assess the extent of electrostatic interactions between protein molecules, it is essential to determine the effective charge of the protein. Recent evidence suggests that the apparent charge on a protein may not reflect the theoretical charge that is expected from the amino acid sequence, but rather can depend on the types and concentrations of ions in solution.[19,20] Several methods have been employed to measure the electrophoretic mobility of proteins in the solutions of interest, from which

the zeta potential, which is the potential at the slipping plane or diffuse layer boundary, can be estimated. These methods include capillary zone electrophoresis (CZE), membrane confined electrophoresis and laser Doppler velocimetry.[19,21,22] The effective charge of a protein, as reflected in the zeta potential, plays a key role in intermolecular interactions.[23]

This work concerns a therapeutic monoclonal antibody (mAb) that exhibits high viscosity and significant opalescence at concentrations above 30 mg/ml, both dependent on the solution conditions. At a typical liquid mAb formulation pH of 6, the ionic strength is the key solution parameter that affects both solution behaviors. Protein-protein intermolecular interactions are evaluated using membrane osmometry and static light scattering in the concentration ranges where opalescence and high viscosity are exhibited. Zeta potentials are measured in order to assess the role of charge repulsion in the intermolecular interactions. A connection between the electrostatic nature of the mAb and viscosity is elucidated. Additionally, the connection between opalescence and critical solution behavior, previously noted by Cromwell et al., is characterized.[7] The dependence of viscosity and opalescence on ionic strength are opposite for this mAb. Furthermore, opalescence reaches a maximum at some mAb concentration and then decreases at higher concentrations. This allows for the simultaneous minimization/optimization of the viscosity and opalescence of the final formulation via intermediate ionic strengths from which a high concentration, self-administered dosage form could be developed.

Materials and Methods

The fully humanized monoclonal antibody of the IgG_1 subclass manufactured by MedImmune Inc, Gaithersburg (USA) will be referred to as the mAb and has a molecular weight of 148 kDa. The sample purity (>99%) was analyzed and confirmed by size exclusion chromatography and gel electrophoresis. Protein concentrations were determined by UV absorption using an extinction coefficient of 1.61 cm^2/mg at 280 nm. All buffer conditions were achieved via exhaustive dialysis which consisted of a minimum of four buffer exchanges over a minimum of 24 hours at volume ratio of buffer to sample of greater than 200:1. The final dialysate was reserved and used for all dilutions, blanks and controls as needed.

Viscosity

Solution viscosities were measured with a Brookfield (Middleboro, MA) model DV-II+ Pro cone/plate viscometer with spindle model CPE-40. The shear rate for all samples with a viscosity below 20 cP was set to 600 s^{-1} (80 RPM); for samples with viscosities above 20 cP a shear rate of 113 s^{-1} (15 RPM) was used. The mAb solution viscosity exhibited little to no dependence on shear rate over the range 10-1000 s^{-1} (data not shown). A solution volume of 0.5 mL was used for all samples and the temperature was controlled at 23°C via a circulating water bath.

In order to interpret the results for the mAb solution viscosity the Mooney hard-sphere viscosity was calculated for an equivalently-sized hard sphere using equation 1.[24]

$$\eta_{hs}=\eta_s \exp\left[\frac{S\Phi}{1-k\Phi}\right] \quad (1)$$

Where, η_{hs} is the viscosity of the equivalent hard-sphere solution, η_s is the viscosity of the solvent, S is a shape parameter, k is a self-crowding factor and Φ represents the volume fraction of the hard-spheres. For these calculations, an S value of 3.6, as determined by Monkos for ovalbumin at room temperature, is used as well as a k value of 1.8 which is independent of temperature.[25]

The experimental viscosity data is fit using the Huggins equation given in equation 2.[26]

$$\eta_{sp}=\frac{\eta}{\eta_s}-1=\eta_{\mathrm{int}}c+K_H\eta_{\mathrm{int}}^2c^2 \quad (2)$$

Where η_{sp} is the specific viscosity, η is the viscosity of the antibody solution, c is the antibody concentration, η_{int} is the intrinsic viscosity and K_H is the Huggins constant.

Opalescence

Opalescence was assessed by nephelometric turbidity which was measured via light scattering at 90° on a spectrofluorometer (SLM AMINCO, Urbana, IL, US) equipped with a temperature-controlled cell holder and 0.2 cm path length quartz cuvette. The excitation and emission were both set to 510 nm with a 4 nm bandwidth. All samples were measured at 23°C and filtered with a Whatman Anotop 0.1 μm filter immediately prior to the measurement. The light scattering intensity was converted to nephelometric turbidity (NTU) using a calibration curve generated from AMCO Clear turbidity standards (GFS Chemicals, Columbus, OH).

Membrane Osmometry

The osmotic pressure of the mAb solutions was measured with a Wescor (Logan, UT) Colloid Osmometer Model 4420. A 10,000 MWCO membrane (product # SS-050) was used with the corresponding dialysate as the reference solution. All measurements were made at room temperature (~23°C). The Osmocoll N standard (product # SS-025) was used for calibration. An initial sample injection of 300 μL followed by a minimum of 2 subsequent 50 μL injections were used until a stable pressure reading was obtained.

To interpret the osmotic pressure data the osmotic virial expansion of the van't Hoff equation is employed.[27]

$$\frac{\Pi}{cRT}=\frac{1}{M_n}+(SVC)\,c \quad (3)$$

Where Π is osmotic pressure, R is the universal gas constant, T is the absolute temperature, M_n is a number-averaged molecular weight, and SVC is the osmotic second virial coefficient. For comparison of the osmotic pressure results to theoretical hard-sphere values the Carnahan-Starling hard-sphere approximation is utilized.[28]

$$\frac{\Pi}{\rho_{hs}k_BT}=\frac{1+\xi+\xi^2-\xi^3}{(1-\xi)^2} \quad (4)$$

$$\xi=\frac{\pi}{6}\rho_{hs}\sigma^3 \quad (5)$$

Where, ρ_{hs} is the number density of hard-spheres k_B is the Boltzman constant, ξ is the effective hard-sphere packing fraction and σ is the effective hard-sphere diameter. The hydrodynamic diameter of for the mAb of 10.2 nm, as measured by dynamic light scattering, was used for the effective hard-sphere diameter.

Light Scattering

Static light scattering is a complementary method to membrane osmometry for determination of the osmotic second virial coefficient. An Electro-Optics laser model 1145AP (Hsintien City, Taiwan), a Brookhaven Instruments goniometer and cascade

photodiode detector model BI-200SM and BI-APD (Holtsville, NY) respectively, were used to determine the excess Rayleigh ratios at a 90° angle (scattering due to protein only) to the incident 633 nm light beam. The relationship used to determine the osmotic second virial coefficient is given here and is derived from the virial expansion of the ideal osmotic pressure equation.[29]

$$\frac{Kc}{R_{90}} = \frac{1}{M_w} + 2\,(SVC)\,c \quad (6)$$

Where M_w is the mass-averaged molecular weight, R_{90} is the excess Rayleigh ratio at 90° and the optical constant K is described by equation 7.

$$K = \frac{4\pi^2 n_0{}^2 (dn/dc)^2}{N_A \lambda^4} \quad (7)$$

Where n_0 is refractive index of the solvent, dn/dc is the refractive index increment and λ is the wavelength of the incident beam. The Rayleigh ratio is given by equation 8.

$$R = \frac{I_\theta r^2}{I_{inc} V_{obs}} = I_\theta\,(constant) \quad (8)$$

Here r is the distance from the observed volume to the detector, I_{inc} is the incident intensity of the laser beam, I_θ is the measured intensity of the scattered light and V_{obs} is the observed volume. A refractive index increment of 0.185 mL/g, estimated from a weight averaged contribution from the protein and carbohydrate portions of the mAb, was used for all light scattering analysis.[30] The constant can be determined from a system for which the Rayleigh ratio is known, in this case toluene at 633 nm ($14*10^{-6}$ cm^{-1}). Once the constant is determined then raw intensity measurements can be converted to Rayleigh ratios and the excess Rayleigh ratio is simply the Rayleigh ratio of the sample minus that of the solvent.

For the dynamic light scattering the same equipment described above was employed as well as a BI-9000AT digital autocorrelator (Brookhaven Instruments, Holtsville, NY). A protein concentration of 1 mg/mL was used for all samples. The resulting correlation functions were used to determine the diffusion coefficients from which the hydrodynamic diameters were calculated by the Stokes equation. The temperature for all light scattering measurements was controlled at 23 °C using a circulating bath temperature controller, and a solvent viscosity of 0.9 cP was used for all hydrodynamic diameter calculations. The mAb's hydrodynamic diameter (10.2 ± 0.8 nm) did not vary significantly with the solvent conditions used in this work.

Zeta Potential

A Malvern Zetasizer Nano ZS (Malvern, UK) was used to measure the electrophoretic mobility of the antibody via laser Doppler velocimetry. The zeta potential is calculated from Henry's equation using the Smoluchoski approximation which is valid for ionic strengths above 1 mM.[22]

$$\mu_e = \frac{2\varepsilon k_s \zeta}{3\eta} \quad (9)$$

Where μ_e is the electrophoretic mobility, ε is the dielectric constant or permittivity of the solution, k_s is a model-based constant which from the Smoluchoski approximation is 1.5 and ζ is the zeta potential. An antibody concentration of 2 mg/mL was used for all samples and

the measurement was repeated on three samples at each condition and the errors are reported as the standard deviation. The temperature was controlled at 23°C.

The effective charge of an equivalent sphere can be estimated via the linearized Poisson-Boltzman equation, also referred to as the Debye-Hückel approximation, and is given by equation 10.[31]

$$Z=\frac{4\pi\varepsilon r_p\,(1+\kappa r_p)\,\zeta}{e} \quad (10)$$

Where Z is the effective charge, r_p is the effective sphere radius, κ is the inverse electric double layer thickness or inverse Debye length and e is the elementary charge.

The electrostatic contribution to the osmotic second virial coefficient, also referred to as the Donnan term can be calculated using equation 11.[16]

$$SVC_{electrostatic}=\frac{Z^2}{4M^2\rho_s m_{ions}} \quad (11)$$

Where $SVC_{electrostatic}$ is the electrostatic component of the second virial coefficient, M is the actual molecular weight of the protein, ρ_s is the solvent density and m_{ions} is the molal concentration of ions.

Results

Viscosity

The mAb viscosity was measured at ionic strengths of approximately 4 and 154 mM (neglecting the contribution of the polyelectrolytic protein); these solution conditions are referred to as low and high ionic strength. From Figure 1 it is clear that the viscosity is much higher in the low ionic strength buffer systems regardless of buffer type; however, the differences in viscosity were only measurable at mAb concentrations above 50 mg/mL. The curves shown in Figure 1 are fits to the Huggins equation (equation 2). Addition of 150 mM NaCl to solutions containing the mAb at concentrations of 80 mg/mL results in an approximately threefold decrease in the solution viscosity. In fact, in the presence of 150 mM NaCl, the solution viscosity is only slightly larger than that predicted for non-interacting hard-spheres via the Mooney approximation (equation 1), and this excess viscosity is apparent only at the highest protein concentrations tested. Finally, the addition of 2 mM NaCl to the 10 mM histidine formulation results in a significant decrease in solution viscosity.

Opalescence

Nephelometric turbidity, a measurement commonly used in determination of water clarity that has been applied to protein opalescence, was utilized to quantify the degree of opalescence.[4] Four of the buffer conditions used for the viscosity measurements were tested for opalescence (Figure 2). To reduce the potential of scattering from insoluble particulates the solutions were passed through a 0.1 μm syringe filter directly into the clean sampling cuvette and the scattering intensity was measured immediately. The high ionic strength solutions are more opalescent than the low ionic strength solutions, although the differences are only apparent at the higher protein concentrations, in this case above 30 mg/mL. This ionic strength dependence is opposite to that observed for the viscosity. There is an approximate threefold increase in opalescence with the addition of 150 mM NaCl to solutions containing 80 mg/mL mAb. To further elucidate the effect of ionic strength, opalescence was measured as a function of mAb concentration in solutions containing 10

mM histidine and either 0, 2, 5, 10 or 150 mM NaCl at a pH of 6 (Figure 5). The ionic strengths of the solutions are 4, 6, 9, 14 and 154 mM NaCl respectively. It is apparent that at the lower ionic strengths (<154 mM NaCl), opalescence reaches a maximum at mAb concentrations in the vicinity 60 mg/mL.

Osmometry and Light Scattering

In order to probe the protein-protein intermolecular interactions in the four solution conditions of interest, osmotic pressure measurements were used to generate osmotic virial plots (Figure 3). Similarly, light scattering intensities at 90° were used to produce the Debye plots (Figure 4). The resulting molecular weights (number-averaged when determined from osmotic pressure measurements and weight-averaged when determined by light scattering) and the osmotic second virial coefficients from the linear regressions of the data are presented in Table 1. All of the measured molecular weights are near that expected for the monomer (148 kDa) and there is little curvature over the concentration range, measured suggesting that the antibody is monomeric and there is not a significant amount of antibody self-association. Additionally, the two low ionic strength buffer conditions generate positive slopes, indicating net pair-wise repulsion between antibody molecules in the corresponding buffer systems. The two high ionic strength buffer conditions result in negative slopes, indicative of net pair-wise attraction between antibody molecules in the given solution. For the net-repulsive conditions the amount of light scattered is near or slightly less than that predicted for a hard-sphere solution of monomers, whereas for the net-attractive conditions the intensity of scattered light is larger than that expected based on hard-sphere predictions. There is approximately a threefold difference in the Rayleigh ratios or intensity of scattered light at 40 mg/mL between the low and high ionic strength solutions for each buffer type.

Zeta Potential and Charge Estimates

To determine the role of electrostatics in the solution behavior of this mAb, zeta potentials were measured for the mAb in the low and high ionic strength buffer systems. The results are presented in Table 2. The antibody in the two low ionic strength solutions exhibits a zeta potential an order of magnitude higher than that observed in the high ionic strength solutions. In fact, the electrophoretic mobility of the mAb in both 150 mM NaCl buffer systems was barely perceptible by the laser Doppler velocimetry technique used, suggesting that the molecule possesses a very low effective charge under these conditions. The effective charge estimates, using the Debye-Hückel approximation (equation 10), are approximately threefold lower in the high ionic strength solutions compared to effective charges in the low ionic strength solutions. Interestingly, the theoretical surface charge for the mAb at pH 6 is +15. Although the zeta potential is still positive, even the 4 mM ionic strength solutions reduce the effective charge at the slipping plane by a factor of 4. The effective charge at the slipping plane or diffuse layer boundary is what contributes to the intermolecular interactions and this can be reflected in the estimate of the electrostatic contribution to the second virial coefficient.[16] The electrostatic contribution to the second virial coefficient is significant for the low ionic strength buffer conditions. In fact, it is on the same order as the difference in the measured second virial coefficients for the mAb at the low and high ionic buffer systems. The electrostatic contribution to the second virial coefficient in the high ionic strength solutions is insignificant when compared to the total second virial coefficient. This that the switch from net-repulsive to net-attractive second virial coefficient values at higher ionic strengths are due to decreases in protein effective charge and increased electrostatic screening of the remaining charge at high ionic strength.

Discussion

Charges on the surface of antibodies result in long-range intermolecular forces that predominate at low ionic strengths and are the primary source of the high solution viscosity. The Debye length at a 4 mM ionic strength is approximately 4.8 nm, whereas the average hydrodynamic surface-to-surface antibody spacing is on the same order, approximately 9 nm at an antibody concentration of 50 mg/mL and 5 nm at 100 mg/mL. This is the primary source of the large increases in viscosity near 100 mg/mL in the low ionic strength solutions. Charge repulsion and the related electric double layer have been noted as the source of high viscosity for proteins and other polyelectrolytes.[32] As the intrinsic fluorescence and far ultra-violet circular dichroism (far UV-CD) signals are unaffected by NaCl for this mAb (data not shown) the mAb conformation appears to be independent of ionic strength. With the assumption that the antibody structure is not significantly affected by ionic strength, there are two main contributions to viscosity which are prevalent at low ionic strengths and are referred to as electroviscous effects. The first is resistance to movement from the double layer surrounding each protein molecule. The concentration of ions in the electric double layer is significantly different than in the bulk solution, the electric double layer then acts as an effective increase in the hydrodynamic radius of the molecule. The second results from the charge repulsion from the double layers of other molecules which is directly related to the zeta potential.

Saluja et al. have shown these electroviscous effects to be important for antibody solutions at low ionic strengths (4 mM) utilizing high-frequency rheology measurements.[33] At ionic strengths above 10 mM the electroviscous effects become less and less significant as the electric double layer becomes more similar to the bulk solution, the effective charge on the protein is reduced and Debye length is shortened due to charge screening. The high ionic strength solution conditions yield viscosities very near those expected for the equivalent hard-spheres. This suggests that the short range van der Waals forces responsible for intermolecular attraction contribute significantly less to the solution viscosity than the long range, repulsive electrostatic forces. It has been reported that reversible association increases antibody solution viscosity;[6,8] however, electrostatic effects were not directly investigated in that work. The conclusion was drawn because the extent of reversible association and the viscosity decreased with increasing ionic strength. The electroviscous effects were not investigated or identified as possible contributors to the reduction in viscosity. The dominant source of the high viscosity for this mAb is repulsive and electrostatic in nature.

Opalescence is a phenomenon of Rayleigh scatters and the increased light scattering of attractive antibody solutions has been attributed to an increased apparent or effective molecular weight.[4] In a recent study of other opalescent mAb formulations, Cromwell et al. demonstrated through measurement of critical exponents, that critical density fluctuations, related to proximity to mixture critical points, result in extensive Rayleigh scattering from monomeric antibody molecules under solution conditions that produce net protein-protein attraction.[7] Opalescence has long been a phenomenon linked to phase behavior near critical points and is thus often referred to as critical opalescence. Some of the earliest work on the relationship between opalescence and critical points was performed in the early 20th century for gases[34] and for homogenous and mixed fluid systems.[35,36] Later in the century the theory was applied to solutions of polymers such as polystyrene.[37,38,39,40] This type of critical behavior was later characterized for protein solutions.[41,42,43] The connecting theme is that density fluctuations, which become more significant or longer in range near the critical point, are the source of the increased light scattering observed as critical opalescence. An eloquent explanation of this effect is offered by Chu and briefly summarized here.[44] Chu explains that the polarizability of a molecule, the property that determines the intensity of light scattered, is dependent on the local density. Furthermore,

any local concentration fluctuations, which become significant near critical points, increase the intensity of light scattered relative to a more ideal system with less significant density fluctuations. The magnitude of the density fluctuations is related to the distance in concentration and temperature space from the critical point, and the closer a given condition is to the critical point, the more pronounced and longer in range the density fluctuations become. It is important to note that critical opalescence can persist some distance away from the critical point. For example, long-range density fluctuations, referred to as off-critical density fluctuations, were observed for a lysozyme-NaCl system away from its critical point.[45]

Since the degree of critical opalescence is determined by the proximity to the critical point, this allows for interesting formulation strategies; two of which are illustrated in Figures 5 and 6. It is obvious that lowering the protein concentration is one strategy to avoid opalescence and viscosity issues; however, this is not desirable for many processing steps or for self-administrable dosage forms. At most of the ionic strengths tested in Figure 5 the opalescence reaches a maximum near 60 mg/mL. This suggests an apparent critical concentration in the vicinity of 60 mg/mL. Thus, at concentrations critical concentration, the distance from the critical point increases with increasing protein concentration, as is suggested from the hypothetical diagram in Figure 6, where the maximum corresponds to the critical concentration. As a result, the intensity of the critical opalescence decreases with increasing protein concentration above the critical point, as predicted in Figure 6B and shown experimentally in Figure 5. The critical point is expected to be sensitive to ionic strength, particularly at the low ionic strengths tested here. Increasing ionic strength appears to increase the critical temperature, whereas the apparent critical concentration does not seem to depend strongly on ionic strength in the range 4-14 mM range. At the relatively high ionic strength of 154 mM, no maximum in opalescence is observed as a function of mAb concentration. This could be due to a shift in the shape of the phase envelope at higher ionic strength or approach of another phase boundary such as the solid/liquid boundary.

Ideally, the exact location of the critical point could be measured as a function of the ionic strength and other solution parameters. However, because in the present case we were unable to observe liquid-liquid phase separation even at temperatures approaching freezing, it is likely that the critical points are near or below the freezing point of water, and therefore are not experimentally accessible.

However, with an understanding of critical solution behavior the protein concentration can be increased above the apparent critical concentration and the solution ionic strength simultaneously can be manipulated to generate solutions optimized to yield minimal opalescence and viscosity. An example of this is given by the 6 mM ionic strength solution (10 mM histidine, 2 mM NaCl) in Figures 1 and 5. At concentrations near 100 mg/mL, the solution viscosity is reduced significantly compared to that of the 4 mM ionic strength solution (10 mM histidine), whereas the opalescence is only slightly higher. Furthermore, as the mAb concentration is increased the difference in opalescence between the 4 and 6 mM ionic strength solutions is minimized.

Whereas critical opalescence is the phenomenon observed near critical points; cloud points are the phenomena associated with phase transitions, which can occur away from the critical point. Cloud point behavior also generates an increase in light scattering which gives a solution an opalescent appearance. However, strictly speaking, once a new macroscopic phase is formed it is no longer an opalescence phenomenon but the more general turbidity of particles larger than Rayleigh scatters. This type of behavior has been characterized for a lysozyme-polyethylene glycol (PEG) system.[46] Because cloud points and mixture critical points may occur in the same vicinity, increased light scattering of antibody solutions could

result from either phase separation or critical phenomena. However, for the mAb described here, no visible phase separation was observed and, as the solutions were filtered immediately prior to the opalescence measurements, it is not likely that the observed phenomenon is a cloud point phenomenon.

As a critical phenomenon, mAb opalescence occurs near phase boundaries. It is known that attractive protein-protein interactions are related to crystalline phase transitions[47] as well as general solubility[48] and liquid-liquid phase separation.[49] Furthermore, the forces that lead to attractive protein-protein interactions are known to be short-range, and often lead to liquid-liquid or other types of phase separation.[18,50] For example, Asherie et al. found that the liquid-liquid phase separation temperature for γIIIb-crystallin increases with increasing degree of oligomerization.[51] In addition to the fact that larger molecules inherently scatter more light, this may be an additional reason antibodies have a greater tendency to generate opalescent solutions than smaller proteins.

The connection between opalescence and phase boundaries is further corroborated by the observation that increasing ionic strength increases both the cloud and crystallization temperatures for lysozyme in both model[52] and experimental systems.[18] A similar conclusion is drawn here as the opalescence increases with increasing ionic strength. Furthermore, the osmotic second virial coefficient for proteins is known to become more attractive with decreasing temperature[53,54] and the opalescence of this mAb increases with decreasing temperature. The nephelometric turbidity increases by 45% upon lowering the temperature from 23°C to 6°C for the 10 mM histidine, 150 mM NaCl solution (data not shown). This is consistent with critical phenomena being responsible for the observed opalescence and it also suggests that the critical temperature is significantly lower than 6°C.

Conclusions

The ionic strength effect on the effective charge of the mAb produces a dramatic effect on the protein-protein interactions that manifest as viscosity and opalescence issues. For this mAb, we observe both high viscosity and significant opalescence in the absence of any significant association/aggregation or particulate formation. Even though the effective charge of the mAb is significantly less than its theoretical value at pH 6, it is still the primary contributor to the intermolecular interactions at low ionic strength. The electrostatic static contribution to the second virial coefficient accounts for the difference in the values at the high and low ionic strengths. This allows for the protein-protein interactions to switch from a net repulsive to a net attractive environment and governs the observed solution behaviors. The increased opalescence of this mAb likely arises from critical density fluctuations. In the low ionic strength formulations the repulsion between mAb molecules reduces the propensity for phase separation and density fluctuations relative to the attractive, higher ionic strength formulations. The lower ionic strength solutions are further from the critical point and thus significantly less light is scattered and the opalescence is reduced.

As the ionic strength and protein concentration can often be altered in a formulation, it should be a useful formulation strategy to balance the repulsive and attractive forces through intermediate ionic strengths. As shown for this mAb, it is possible generate solutions which simultaneously exhibit minimized opalescence and viscosity, even at mAb concentrations near 100 mg/mL.

Acknowledgments

We would like to thank the following people from MedImmune for helpful discussions and support of this work: Stephen Chang, Ambarish Shah, Tom Leach, and Roja Anandakumar, and Cindy Oliver.

References

1. Shire SJ, Shahrokh Z, Liu J. Challenges in the development of high protein concentration formulations. J Pharm Sci. 2004; 93:1390–1402. [PubMed: 15124199]
2. Stockwin LH, Holmes S. Antibodies as therapeutic agents: Vive la renaissance! Expert Opin Biol Ther. 2003; 3:1133–1152. [PubMed: 14519077]
3. Alford JR, Kendrick BS, Carpenter JF, Randolph TW. High concentration formulations of recombinant human interleukin-1 receptor antagonist: II. aggregation kinetics. J Pharm Sci. 2008; 97:3005–3021. [PubMed: 17924426]
4. Sukumar M, Doyle BL, Combs JL, Pekar AH. Opalescent appearance of an IgG1 antibody at high concentrations and its relationship to noncovalent association. Pharm Res. 2004; 21:1087–1093. [PubMed: 15290846]
5. Harris RJ, Shire SJ, Winter C. Commercial manufacturing scale formulation and analytical characterization of therapeutic recombinant antibodies. Drug Dev Res. 2004; 61:137–154.
6. Liu J, Nquyen MDH, Andya JD, Shire SJ. Reversible self-association increases the viscosity of a concentrated monoclonal antibody in aqueous solution. J Pharm Sci. 2005; 94:1928–1940. [PubMed: 16052543]
7. Cromwell, MEM.; Carpenter, JF.; Scherer, T.; Randolph, TW. Opalescence in antibody formulations is a solution critical phenomenon.. 236th ACS National Meeting; Philadelphia, PA, United States. 2008. Abstracts of Papers
8. Kanai S, Liu J, Patapoff TW, Shire SJ. Reversible self-association of a concentrated monoclonal antibody solution mediated by Fab-Fab interaction that impacts solution viscosity. J Pharm Sci. 2008; 97:4219–4227. [PubMed: 18240303]
9. Moon YU, Curtis RA, Anderson CO, Blanch HW, Prausnitz JM. Protein-Protein interactions in aqueous ammonium sulfate solutions. Lysozyme and Bovine Serum Albumin (BSA). J Solution Chem. 2000; 29:699–717.
10. Yousef MA, Datta R, Rodgers VGJ. Understanding Nonidealities of the Osmotic Pressure of Concentrated Bovine Serum Albumin. J Colloid Interface Sci. 1998; 207:273–282. [PubMed: 9792770]
11. Minton AP. A molecular model for the dependence of the osmotic pressure of bovine serum albumin upon concentration and pH. Biophys Chem. 1995; 57:65–70. [PubMed: 8534837]
12. Minton AP. The effective hard particle model provides a simple, robust, and broadly applicable description of nonideal behavior in concentrated solutions of bovine serum albumin and other nonassociating proteins. J Pharm Sci. 2007; 96:3466–3469. [PubMed: 17588257]
13. Minton AP. Effective hard particle model for the osmotic pressure of highly concentration binary protein solutions. Biophys J. 2008; 94:L57–L59. [PubMed: 18212007]
14. Ross PD, Minton AP. Hard quasispherical model for the viscosity of hemoglobin solutions. Biochem Biophys Res Commun. 1977; 76:971–976. [PubMed: 20088]
15. Yousef MA, Datta R, Rodgers VGJ. Free-solvent model of osmotic pressure revisited: application to concentrated IgG solution under physiological conditions. J Colloid Interface Sci. 1998; 197:273–282. [PubMed: 9792770]
16. Asthagiri D, Paliwal A, Abras D, Lenhoff AM, Paulaitis ME. Light-scattering studies of protein solutions: role of hydration in weak protein-protein interactions. Biophys J. 2005; 89:1564–1573. [PubMed: 15980182]
17. Deszczynski M, Harding SE, Winzor DJ. Negative second virial coefficients as predictors of protein crystal growth: evidence from sedimentation equilibrium studies that refutes the designation of those light scattering parameters as osmotic virial coefficients. Biophys Chem. 2006; 120:106–113. [PubMed: 16300875]
18. Broide ML, Tominc TM, Saxowsky MD. Using the phase transitions to investigate the effect of salts on protein interactions. Phys Rev E. 1996; 53:6325–6335.
19. Winzor DJ, Jones S, Harding SE. Determination of protein charge by capillary zone electrophoresis. Anal Biochem. 2004; 333:225–229. [PubMed: 15450796]
20. Winzor DJ. Determination of the net charge (valence) of a protein: a fundamental but elusive parameter. Anal Biochem. 2004; 325:1–20. [PubMed: 14715279]

21. Durant JA, Chen C, Laue TM, Moody TP, Allison SA. Use of T4 lysozyme charge mutants to examine electrophoretic models. Biophys Chem. 2002; 101-102:593–609. [PubMed: 12488029]
22. Faude A, Zacher D, Müller E, Böttinger H. Fast determination of conditions for maximum dynamic capacity in cation-exchange chromatography of human monoclonal antibodies. J Chromatogr A. 2007; 1161:29–35. [PubMed: 17442329]
23. Verway, EJW.; Overbeek, JTG. Theory of the Stability of Lyophobic Colloids. Dover Publications, Inc.; Mineola, New York: 1948.
24. Mooney M. The viscosity of a concentrated suspension of spherical particles. J Colloid Sci. 1951; 6:162–70.
25. Monkos K. Viscosity analysis of the temperature dependence of the solution conformation of ovalbumin. Biophys Chem. 2000; 85:7–16. [PubMed: 10885394]
26. Huggins ML. The viscosity of dilute solutions of long-chain molecules. IV. Dependence on concentration. J Am Chem Soc. 1942; 64:2716–18.
27. Prausnitz, JM.; Lichtenthaler, RN.; Gomez de Azevedo, E. Molecular Thermodynamics of Fluid-Phase Equilibria. Prentice Hall PTR; Upper Saddle River, New Jersey: 1999.
28. Carnahan NF, Starling KE. Equation of state for nonattracting rigid spheres. J Chem Phys. 1969; 51:635–636.
29. Kratochvil, P. Classical Light Scattering for Polymer Solutions. Elsevier; Amsterdam, Netherlands: 1987.
30. Arakawa T, Wen J. Determination of carbohydrate contents from excess light scattering. Anal Biochem. 2001; 299:158–161. [PubMed: 11730337]
31. Chun M, Lee I. Rigorous estimation of effective protein charge from experimental electrophoretic mobilities for proteomics analysis using microchip electrophoresis. Colloids Surf A. 2008; 318:191–198.
32. Harding SE. The intrinsic viscosity of biological macromolecules. Progress in measurement, interpretation and application to structure in dilute solution. Prog Biophys Molec Biol. 1997; 68:207–262. [PubMed: 9652172]
33. Saluja A, Badkar AV, Zeng DL, Nema S, Kalonia DS. Application of High-Frequency Rheology Measurements for Analyzing Protein–Protein Interactions in High Protein Concentration Solutions Using a Model Monoclonal Antibody (IgG2). J Pharm Sci. 2004; 95:1967–1983. [PubMed: 16847932]
34. Smoluchowski M. Molecular kinetic theory of opalescence of gases in their critical region and of some allied phenomenon. Annalen der Physik. 1908; 25:205–226.
35. Einstein A. Theory of the opalescence of homogenous fluids and fluid mixtures in the neighbourhood of the critical state. Annalen der Physik. 1910; 33:1275–1298.
36. Einstein A. Theory of the opalescence of homogeneous and of mixed liquids in the neighborhood of the critical region. Annalen der Physik. 1911; 33:1275–98.
37. Debye P, Chu B, Woermann D. Critical opalescence of polystyrene in cyclohexane: range of molecular forces and radius of gyration. J Chem Phys. 1962; 36:1803–1808.
38. de Gennes PG. Critical opalescence of macromolecular solutions. Phys Lett. 1968; 26A:313–314.
39. Chu B. Comments of critical opalescence of macromolecular solutions. Phys Lett. 1969; 28A:654–655.
40. Vrij A, van den Ester MWJ. Critical opalescence of polymer solutions. J Chem Soc Faraday Trans 2. 1972; 68:513–525.
41. Ishimoto C, Tanaka T. Critical behavior of a binary mixture of protein and salt water. Phys Rev Lett. 1977; 39:474–477.
42. Thomson JA, Schurtenberger P, Thurston GM, Benedek GB. Binary liquid phase separation and critical phenomena in a protein/water solution. Proc Natl Acad Sci USA. 1987; 84:7079–7083. [PubMed: 3478681]
43. Schurtenberger P, Chamberlin RA, Thurston GM, Thomson JA, Benedek GB. Observation of critical phenomenon in a protein-water solution. Phys Rev Lett. 1989; 63:2064–2067. [PubMed: 10040753]
44. Chu B. Critical opalescence and the macromolecule. Adv Macromolecular Chem. 1970; 2:89–120.

45. Manno M, Xiao C, Bulone D, Martorana V, San Biagio PL. Thermodynamic instability in supersaturated lysozyme solutions: Effect of salt and role of concentration fluctuations. Phys Rev E. 2003; 68:011904–1-011904-11.

46. Bloustine J, Virmani T, Thurston GM, Fraden S. Light scattering and phase behavior of lysozyme-poly(ethylene glycol) mixtures. Phys Rev Lett. 2006; 96:087803–1-4. [PubMed: 16606227]

47. George A, Wilson WW. Predicting protein crystallization from a dilute solution property. Acta Crystallogr. 1994; D50:361–365.

48. Demoruelle K, Guo B, Kao S, McDonald MM, Nikic DB, Holman SC, Wilson WW. Correlation between the osmotic second virial coefficient and solubility for equine serum albumin and ovalbumin. Acta Crystallogr. 2002; D58:1544–1548.

49. Dumetz AC, Chockla AM, Kaler EW, Lenhoff AM. Protein phase behavior in aqueous solutions: crystallization, liquid-liquid phase separation, gels and aggregates. Biophy J. 2008; 94:570–583.

50. Annunziata O, Asherie N, Lomakin A, Pande J, Ogun O, Benedek GB. Effect of polyethylene glycol on the liquid–liquid phase transition in aqueous protein solutions. Proc Natl Acad Sci USA. 2002; 99:14165–14170. [PubMed: 12391331]

51. Asherie N, Pande J, Lomakin A, Ogun O, Hanson SRA, Smith JB, Benedek GB. Oligomerization and phase separation in globular protein solutions. Biophys Chem. 1998; 75:213–227. [PubMed: 9894340]

52. Pellicane G, Costa D, Caccamo C. Cloud and solubility temperatures versus ionic strength in model lysozyme solutions. J Phys Condens Matter. 2003; 15:S3485–S3489.

53. Gripon C, Legrand L, Rosenman I, Vidal O, Robert MC, Boub F. Lysozyme-lysozyme interactions in under- and super-saturated solutions: a simple relation between the second virial coefficients in H20 and D20. J Cryst Growth. 1997; 178:575–584.

54. Pellicane G, Costa D, Caccamo C. Phase coexistence in a DLVO model of globular protein solutions. J Phys Condens Matter. 2003; 15:375–384.

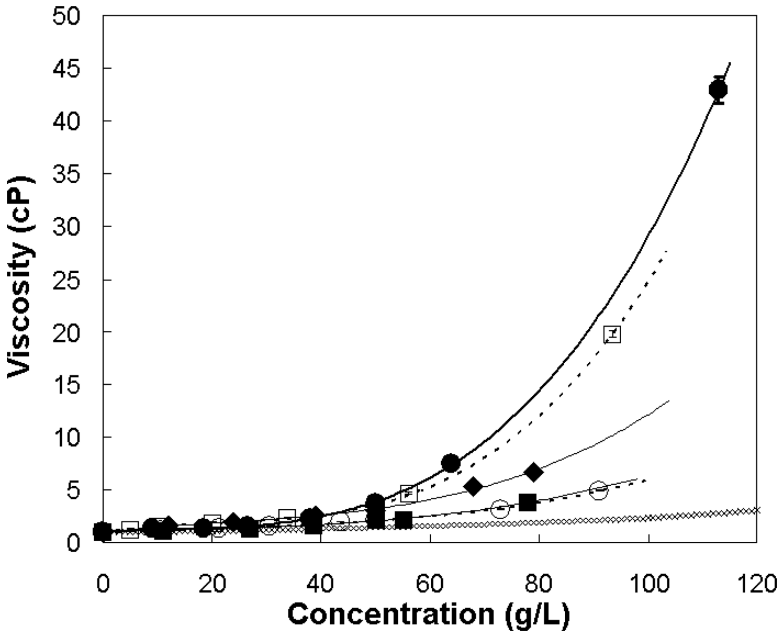

Figure 1.

The concentration dependence of the viscosities of the mAb solutions at pH 6 and two ionic strengths. Solution conditions are: (●) 10 mM histidine, (□) 2.2 mM sodium phosphate, (○) 10 mM histidine, 150 mM NaCl, (■) 2.2 mM sodium phosphate, 150 mM NaCl, (◆) 10 mM histidine, 2 mM NaCl, (◇) Viscosity of an equivalent hard-sphere using the Mooney approximation (Equation 1). Lines represent a fit to the polynomial in Equation 2 where the solid lines correspond to the closed symbols and the dashed lines correspond to the open symbols. Error bars represent standard deviation from three samples.

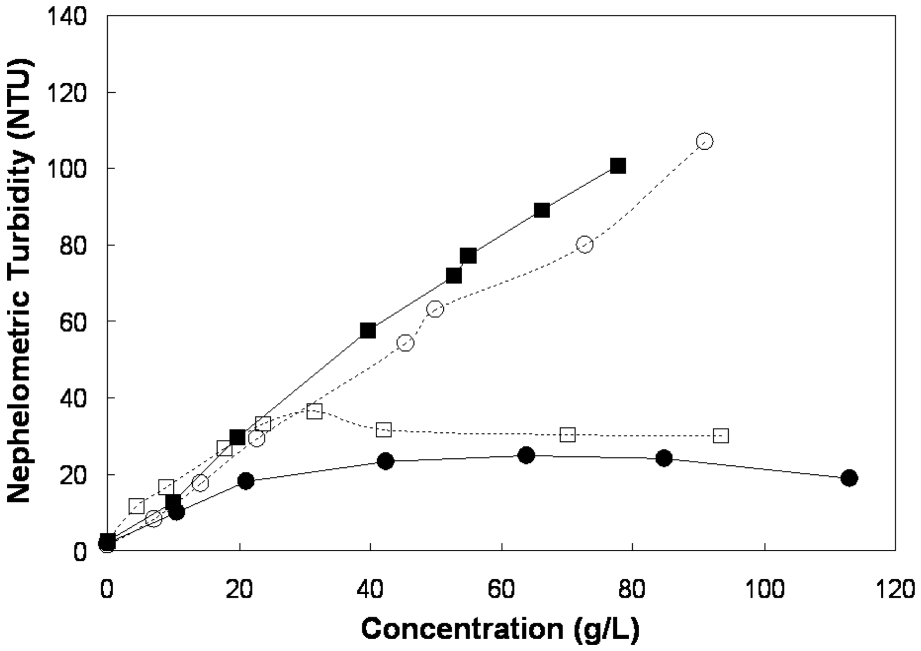

Figure 2.

Opalescence, measured by nephelometric turbidity, as a function of the mAb concentration at pH 6. Solution conditions are: (●) 10 mM histidine, (□) 2.2 mM sodium phosphate, (○) 10 mM histidine, 150 mM NaCl, (■) 2.2 mM sodium phosphate, 150 mM NaCl. Lines are to guide the eye. Error bars from triplicate samples are smaller than the data points.

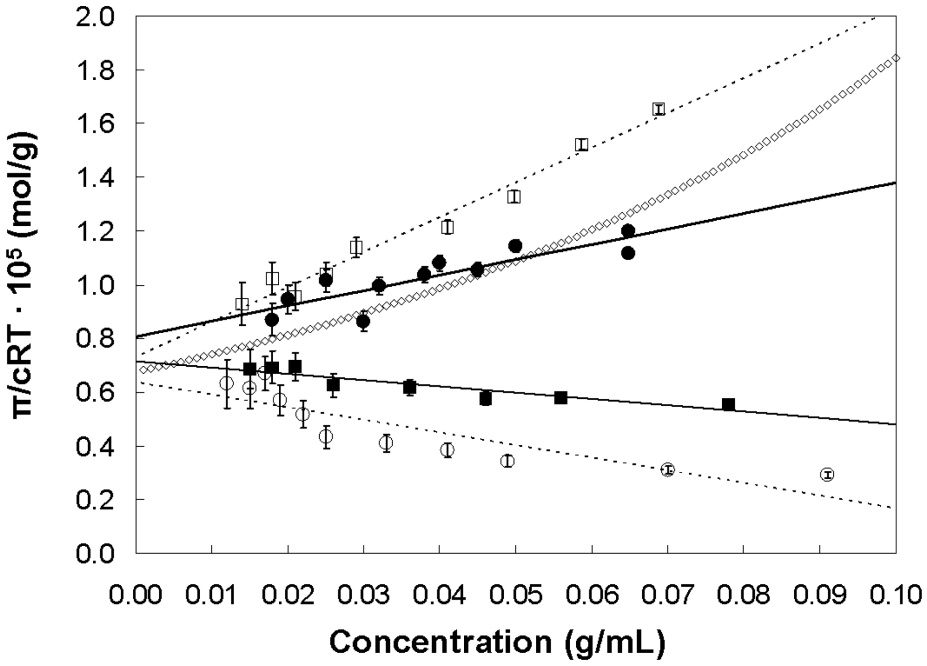

Figure 3.

Osmotic pressure of the mAb at pH 6 measured by membrane osmometry. (●) 10 mM histidine, (□) 2.2 mM sodium phosphate, (○) 10 mM histidine, 150 mM NaCl, (■) 2.2 mM sodium phosphate, 150 mM NaCl, (◇) Predicted osmotic pressure of an equivalent hard-sphere using the Carnahan-Starling approximation with a hard-sphere radius equal to the hydrodynamic radius of the mAb of 5.1 nm (Equation 5). Remaining lines are linear regressions of the corresponding data sets and the short dashed lines correspond to the open symbols. Error bars corresponds to ±0.2 mmHg which is the specified sensitivity limit of the osmometer and is typically larger than the sample to sample variation.

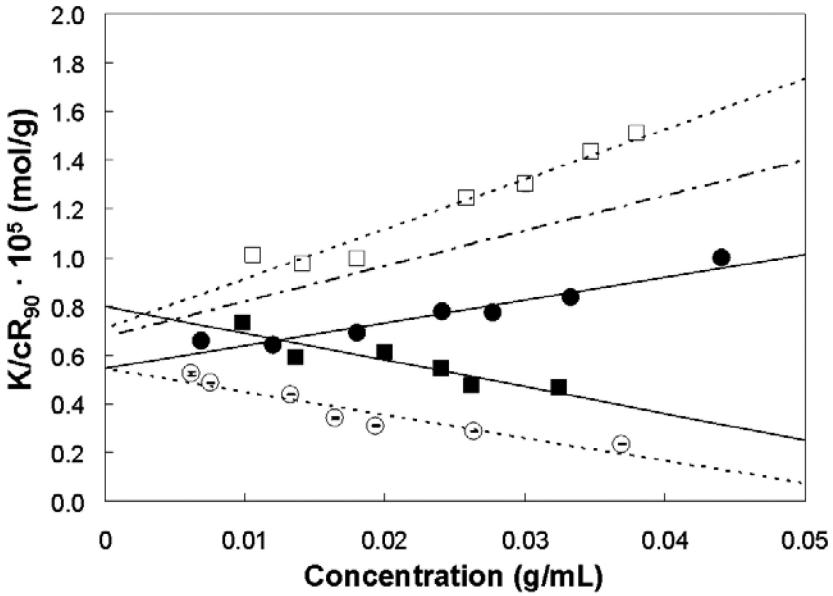

Figure 4.

Debye plot generated from light scattering measurements of the mAb at pH 6 in various solutions. (●) 10 mM histidine, (□) 2.2 mM sodium phosphate, (○) 10 mM histidine, 150 mM NaCl, (■) 2.2 mM sodium phosphate, 150 mM NaCl. The long dash, short dash line represents the predicted light scattering from an equivalent hard-sphere with a radius equivalent to the hydrodynamic radius of the mAb of 5.1 nm. Remaining lines are linear regressions of the corresponding data sets and the dotted lines correspond to the open symbols. Error bars represent standard deviation for three measurements.

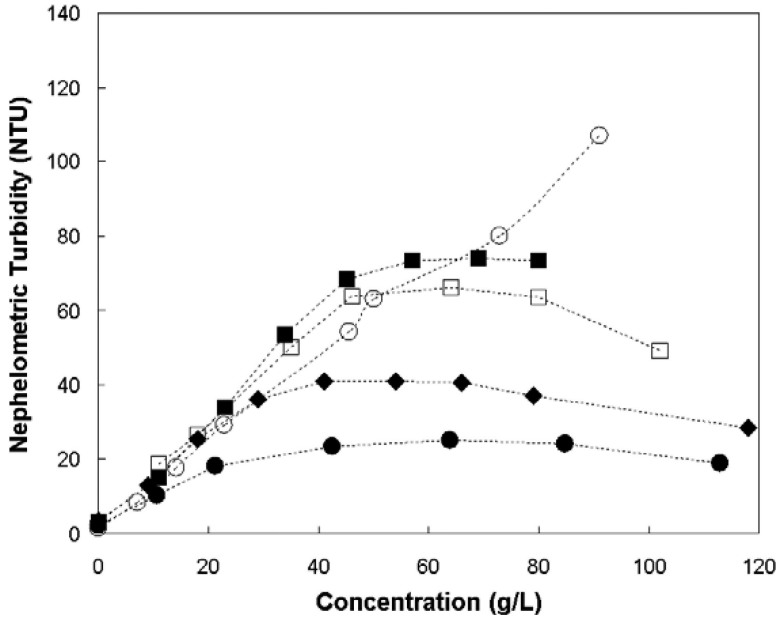

Figure 5.

The effect of ionic strength on mAb opalescence at pH 6. Where the opalescence is measured by nephelometric turbidity, and the ionic strength is adjusted with NaCl. Solution conditions are: (●) 10 mM histidine ionic strength = 4 mM, (◆) 10 mM histidine, 2 mM NaCl, ionic strength = 6 mM (□) 10 mM histidine, 5 mM NaCl, ionic strength = 9 mM (■) 10 mM histidine, 10 mM NaCl, ionic strength = 14 mM (○) 10 mM histidine, 150 mM NaCl, ionic strength = 154 mM. Lines are to guide the eye. Error bars from triplicate samples are smaller than the data points.

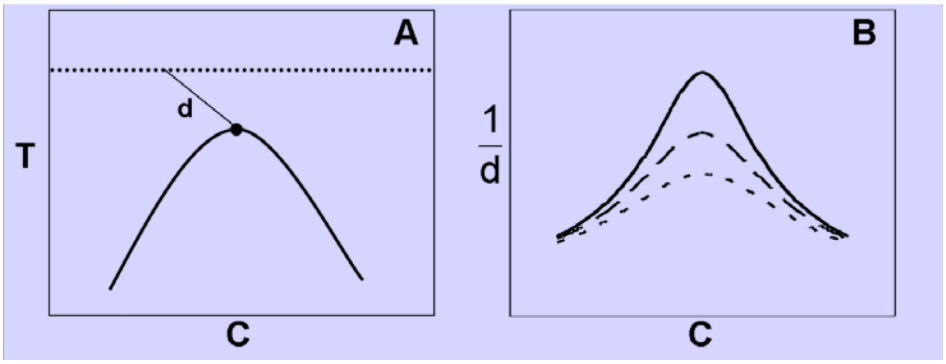

Figure 6.

Panel A – Hypothettical liquid-liquid phase separation boundary (solid bold curve). The dotted line represents an isotherm above the critical temperature.. The dot represents the critical point at some critical temperature, T_c and concentration, C_c. The connecting line represents the distance (d) from the isotherm to the critical point. Panel B – The inverse of the calculated distance, which is directly related to the extent of critical opalescence as a function of the concentration. In both panels, solid and dashed lines represent hypothetical phase envelopes.d

Table 1

Second virial coefficients (SVC) and molecular weights are reported as determined by linear regression of the data in Figures 3 and 4. All measurements were conducted at a pH of 6. Units of the SVC are $mL \cdot mol/g^2$ and the units of MW are kDa. Errors represent 95% confidence intervals from the regressions.

	Osmometry		Light Scattering	
Formulation	**SVC × 10^5**	**MW**	**SVC × 10^5**	**MW**
10 mM Histidine	5.76 ± 2.51	124 ± 17	4.93 ± 0.65	174 ± 10
2.2 mM Sodium Phosphate	13.0 ± 1.9	137 ± 14	10.2 ± 1.2	141 ± 13
10 mM Histidine, 150 mM NaCl	−4.30 ± 2.02	163 ± 21	−4.71 ± 0.89	174 ± 11
2.2 mM Sodium Phosphate, 150 mM NaCl	−2.36 ± 1.08	140 ± 9	−4.98 ± 1.31	125 ± 9

Table 2

The measured zeta potentials for the mAb in the four buffer conditions of interest at pH 6, as well as the corresponding calculations of effective charge and the electrostatic component of the second virial coefficient (SVC). The units of zeta potential are mV and the units of SVC are mL·mol/g^2. Errors represent standard deviation from three measurements.

Formulation	zeta potential (mV)	effective charge	$SVC_{electrostatic} \times 10^5$ (mL·mol/g^2)
10 mM Histidine	7.40 ± 0.41	3.83	6.82
2.2 mM Sodium Phosphate	6.93 ± 0.32	3.56	6.80
10 mM Histidine, 150 mM NaCl	0.55 ± 0.86	1.12	0.00952
2.2 mM Sodium Phosphate, 150 mM NaCl	0.56 ± 0.85	1.13	0.00976